

# A bias-corrected GEMS geostationary satellite product for nitrogen dioxide using machine learning to enforce consistency with the TROPOMI satellite instrument

Yujin J. Oak<sup>1</sup>, Daniel J. Jacob<sup>1,2</sup>, Nicholas Balasus<sup>1</sup>, Laura H. Yang<sup>1</sup>, Heesung Chong<sup>3</sup>, Junsung Park<sup>3</sup>,  
5 Hanlim Lee<sup>4</sup>, Gitaek T. Lee<sup>5</sup>, Eunjo S. Ha<sup>5</sup>, Rokjin J. Park<sup>5</sup>, Hyeong-Ahn Kwon<sup>6</sup>, Jhoon Kim<sup>7</sup>

<sup>1</sup>School of Engineering and Applied Sciences, Harvard University, Cambridge, MA, USA

<sup>2</sup>Department of Earth and Planetary Sciences, Harvard University, Cambridge, MA, USA

<sup>3</sup>Harvard-Smithsonian Center for Astrophysics, Cambridge, MA, USA

10 <sup>4</sup>Division of Earth Environmental System Science, Major of Spatial Information Engineering, Pukyong National University, Busan, South Korea

<sup>5</sup>School of Earth and Environmental Science, Seoul National University, Seoul, South Korea

<sup>6</sup>Department of Environmental and Energy Engineering, University of Suwon, Suwon, South Korea

<sup>7</sup>Department of Atmospheric Sciences, Yonsei University, Seoul, South Korea

Correspondence to: Yujin J. Oak (yjoak@g.harvard.edu)

15 **Abstract.** The Geostationary Environment Monitoring Spectrometer (GEMS) launched in February 2020 is now providing continuous daytime hourly observations of nitrogen dioxide (NO<sub>2</sub>) columns over East Asia (5°S–45°N, 75°E–145°E) with 3.5 × 7.7 km<sup>2</sup> pixel resolution. These data provide unique information to improve understanding of the sources, chemistry, and transport of nitrogen oxides (NO<sub>x</sub>) with implications for atmospheric chemistry and air quality, but opportunities for direct validation are very limited. Here we correct the operational level-2 (L2) NO<sub>2</sub> vertical column densities (VCDs) from  
20 GEMS with a machine learning (ML) model to match the much sparser but more mature observations from the low Earth orbit TROPospheric Monitoring Instrument (TROPOMI), preserving the data density of GEMS but making them consistent with TROPOMI. We first reprocess the GEMS and TROPOMI operational L2 products to use common prior vertical NO<sub>2</sub> profiles (shape factors) from the GEOS-Chem chemical transport model. This removes a major inconsistency between the two satellite products and greatly improves their agreement with ground-based Pandora NO<sub>2</sub> VCD data in source regions.  
25 We then apply the ML model to correct the remaining differences, Δ(GEMS-TROPOMI), using as predictor variables the GEMS NO<sub>2</sub> VCDs and retrieval parameters. We train the ML model with collocated GEMS and TROPOMI NO<sub>2</sub> VCDs, taking advantage of TROPOMI off-track viewing to cover the wide range of effective zenith angles (EZAs) ~~observed by~~  
GEMS. The two most important predictor variables for Δ(GEMS-TROPOMI) are GEMS NO<sub>2</sub> VCD and EZA. The corrected GEMS product is unbiased relative to TROPOMI and shows a diurnal variation over source regions more consistent with  
30 Pandora than the operational product.

Deleted: for the GEMS diurnal profiles

## 1 Introduction

Nitrogen oxides ( $\text{NO}_x \equiv \text{NO} + \text{NO}_2$ ) are reactive trace gases emitted from combustion, lightning, and microbial activity in soils. Emission is mainly as nitrogen oxide (NO) which cycles rapidly with nitrogen dioxide ( $\text{NO}_2$ ). This cycling produces tropospheric ozone ( $\text{O}_3$ ) and oxidation of  $\text{NO}_x$  produces nitrate particulate matter (PM), with implications for air quality, climate forcing, and nitrogen deposition. Satellite measurements of  $\text{NO}_2$  vertical column densities (VCDs) by solar backscatter from polar sun-synchronous low Earth orbit (LEO) have been used extensively to monitor  $\text{NO}_x$  emissions and their trends worldwide (Martin et al., 2003; Lamsal et al., 2015; Curier et al., 2014; Duncan et al., 2016; Liu et al., 2017) and to improve understanding of  $\text{NO}_x$  oxidation chemistry (Boersma et al., 2008; Valin et al., 2013; Miyazaki et al., 2017; Beirle and Wagner, 2024).

$\text{NO}_2$  has been measured continuously from LEO since 1995, starting with the Global Ozone Monitoring Experiment (GOME) (Burrows et al., 1999) followed by the operational GOME-2 series (Munro et al., 2016). The Ozone Monitoring Instrument (OMI) was launched in 2004 and is providing global daily continuous data at  $13 \times 24 \text{ km}^2$  nadir resolution (Levelt et al., 2006). The TROPOspheric Monitoring Instrument (TROPOMI) launched onboard the Sentinel-5 Precursor (S5P) satellite in 2017 improved the resolution to  $3.5 \times 5.5 \text{ km}^2$  (Veeffkind et al., 2012).

OMI and TROPOMI retrievals of  $\text{NO}_2$  have been extensively validated using ground-based measurements of  $\text{NO}_2$  VCDs from sun-staring Pandora spectrometers and Multi-Axis Differential Optical Absorption Spectroscopy (MAX-DOAS) instruments, and also by intercomparisons with each other (Herman et al., 2019; Pinardi et al., 2020; Wang et al., 2020; Cai et al., 2022; Gu et al., 2023). TROPOMI  $\text{NO}_2$  is routinely validated against Pandora, MAX-DOAS, and OMI by the Royal Netherlands Meteorological Institute (KNMI), showing overall good agreement with a  $-7\%$  mean bias (Lambert et al., 2023). It has been used to quantify  $\text{NO}_x$  emissions (Goldberg et al., 2019), infer surface  $\text{NO}_2$  concentrations (Cooper et al., 2020), and evaluate air quality models (Douros et al., 2023).

A limitation with polar sun-synchronous LEO satellites is that they observe a given location at most once per day and at the same time of day. Geostationary satellites can observe at much higher frequency and in principle continuously, providing much denser data and a unique capability for tracking the diurnal cycle of emissions, oxidation chemistry, and pollutant transport. The Geostationary Environment Monitoring Spectrometer (GEMS) was launched onboard the Korea Aerospace Research Institute GEO-KOMPSAT2B (GK2B) satellite in February 2020, in an equatorial plane at  $128.2^\circ$ -longitude with continuous view of East Asia at  $3.5 \times 7.7 \text{ km}^2$  pixel resolution over Korea (Kim et al., 2020). It is now providing the first  $\text{NO}_2$  observations from geostationary orbit. GEMS is part of a geostationary air quality constellation to include TEMPO over North America launched in April 2023 (Zoogman et al., 2017) and Sentinel-4 over Europe to be launched in 2025 (Ingmann et al., 2012).

As with all satellite observations, GEMS retrievals take some time to mature.  $\text{NO}_2$  VCDs (L2 products) are currently retrieved operationally with the version 2.0 algorithm (National Institute of Environmental Research, 2020). Evaluation of the GEMS  $\text{NO}_2$  product with four urban Pandora observations in South Korea found an underestimate and disagreements in

65 diurnal patterns (Kim et al., 2023). However, the local Pandora data may not be representative of the  $3.5 \times 7.7$  km<sup>2</sup> GEMS  
pixels particularly in urban environments. GEMS evaluation for China found both high and low biases in comparison with  
ground-based observations and other satellite products (Li et al., 2023; Zhang et al., 2023). Yang et al. (2024) reprocessed  
the GEMS NO<sub>2</sub> version 2.0 data with prior NO<sub>2</sub> vertical profiles from the GEOS-Chem chemical transport model (CTM) on  
a  $0.25^\circ \times 0.3125^\circ$  grid and found good agreement with Pandora in Seoul and Beijing including diurnal variations.

70 Here we introduce a bias-corrected GEMS NO<sub>2</sub> product using machine learning (ML) to minimize the biases between  
GEMS and TROPOMI, and provide in this manner a more reliable and consistent satellite product for scientific applications  
and for improving the GEMS retrieval. Although TROPOMI observes over a limited range of solar zenith angles (SZAs) on  
account of the overpass time at approximately 13:30 local time (LT), it has off-track viewing to  $\pm 50^\circ$  providing a range of  
viewing zenith angles (VZAs) to mimic the wider range of SZAs seen by GEMS. The bias-corrected GEMS product  
75 combines the high data density of GEMS with the accuracy of TROPOMI demonstrated by extensive validation and  
algorithm development (Gu et al., 2023; Eskes et al., 2022). Our approach is as follows. First, we adjust for biases caused by  
different prior information used in the operational L2 retrievals by applying common prior vertical profiles simulated by  
GEOS-Chem. Second, we train an ML model using GEMS and TROPOMI NO<sub>2</sub> VCDs to minimize differences in collocated  
data during 2022–2023 using GEMS retrieval parameters as explanatory variables. Third, we apply the trained ML model to  
80 the ensemble of GEMS data for July 2022–June 2023, producing a bias-corrected GEMS product which has the temporal  
coverage of GEMS and is consistent with TROPOMI. We use the ML model to identify the GEMS retrieval parameters  
associated with the largest discrepancies with TROPOMI and validate this bias-corrected GEMS product with ground-based  
observations from the Pandora spectrometers.

## 2 GEMS, TROPOMI, and Pandora operational products

85 GEMS is an ultraviolet (UV)-visible (VIS) hyperspectral imaging spectrometer that measures solar backscatter with 0.6 nm  
spectral resolution over East Asia ( $5\text{--}45^\circ$  latitude,  $75\text{--}145^\circ$  longitude) with  $3.5 \times 7.7$  km<sup>2</sup> pixels at  $37.5^\circ$ -latitude and hourly  
repeat times (08:45–17:45 LT) (Kim et al., 2020). Total NO<sub>2</sub> slant column densities (SCDs) along the sun-satellite light path  
are retrieved using differential optical absorption spectroscopy (DOAS) (Platt, 1994) with a fitting window of 435–450 nm  
(National Institute of Environmental Research 2020b; Kim et al., 2020). We use the operational L2 product from version 2.0  
90 (available online: <https://nesc.nier.go.kr/en/html/index.do>, last access: 19 January 2024).

TROPOMI is similarly a UV-VIS hyperspectral imaging spectrometer with a full width at half maximum (FWHM) of 0.55  
nm. It is a push-broom instrument with a wide swath of  $\sim 2600$  km and an off-track viewing angle of  $\pm 50^\circ$  off-nadir,  
providing global daily viewing once a day at approximately 13:30 LT with  $5.5 \times 3.5$  km<sup>2</sup> nadir spatial resolution. Total NO<sub>2</sub>  
SCDs are retrieved using DOAS in the 405–465 nm window (van Geffen et al., 2022). Here we use the offline (OFFL) L2  
95 product produced by the KNMI NO<sub>2</sub> processor version 2.4.0 (available online: [https://dataspace.copernicus.eu/explore-  
data/data-collections/sentinel-data/sentinel-5p](https://dataspace.copernicus.eu/explore-data/data-collections/sentinel-data/sentinel-5p), last access: 19 January 2024).

Ground-based NO<sub>2</sub> column measurements from Pandora instruments have been widely used to validate satellite retrievals (Park et al., 2022; Kim et al., 2023; Pinardi et al., 2020; Yang et al., 2024). Pandora spectrometers provide direct-sun observations to retrieve ground-based NO<sub>2</sub> VCDs by DOAS using a spectral fitting window of 400–470 nm (Herman et al., 2009). Here we use the L2 total NO<sub>2</sub> VCDs processed by the BlickP software (available online: <https://www.pandonia-global-network.org>, last access: 19 January 2024) at 16 Pandora stations located in Northeast Asia (China, South Korea, Japan) from the Pandonia Global Network (PGN). We select data with quality flags of 0, 1, 10, or 11, and with SZA ≤ 70°.

### 3 Reprocessing of GEMS and TROPOMI retrievals to use common vertical profiles

Spectral fitting of satellite solar backscatter observations yields NO<sub>2</sub> SCDs, which must be converted to VCDs (the appropriate geophysical quantity) using air mass factors (AMF = SCD/VCD) (Palmer et al., 2001). Standard retrieval algorithms separate the stratospheric and tropospheric portions of the total VCDs to account for the NO<sub>2</sub> background in the stratosphere from oxidation of nitrous oxide (N<sub>2</sub>O) (Bucsela et al., 2013), but this introduces uncertainty related to the stratosphere-troposphere separation (STS) algorithm which may differ between retrievals (Geddes et al., 2018) and leads to ambiguity in the allocation of near-tropopause NO<sub>2</sub> such as from lightning and aircraft (Travis et al., 2016; Dang et al., 2023). Since the stratospheric background component is readily predictable from CTMs such as GEOS-Chem (Knowland et al., 2022) and the spatial structure in the NO<sub>2</sub> column is mainly from the troposphere, the purpose for separating stratosphere and troposphere is in fact not clear. We focus here on total NO<sub>2</sub> VCDs as most useful for scientific applications and to avoid STS errors.

The AMF from the surface to the top of the atmosphere (TOA) can be decomposed into two parts, scattering weights and vertical shape factors, as follows:

$$\text{AMF} = \int_0^{\text{TOA}} w(z)S(z)dz, \quad (1)$$

where  $w(z)$  is the scattering weight at altitude  $z$  measuring the sensitivity of the instrument to NO<sub>2</sub> at altitude  $z$  as computed by a radiative transfer model (RTM), and  $S(z)$  is the vertical shape factor of normalized number densities obtained from a CTM. Scattering weights for a given wavelength depend on SZA, VZA, relative azimuth angle, surface albedo, and cloud and aerosol optical depths and vertical distributions (Kwon et al., 2019; Hong et al., 2017). The operational GEMS retrieval algorithm uses a look-up-table (LUT) of pre-calculated scattering weights from the VLIDORT RTM at 441 nm (Spurr and Christi, 2014). TROPOMI retrievals use a LUT from the Doubling-Adding KNMI (DAK) RTM at 437.5 nm (Stammes, 2001).

The vertical shape factor  $S(z)$  in Eq. (1) describes how NO<sub>2</sub> is distributed with altitude as determined by emissions, chemistry, and transport. It must be prescribed in the retrieval as independent information. The L2 GEMS and TROPOMI retrievals use normalized partial column densities simulated for the local scene by GEOS-Chem (Bey et al., 2001; Yang et al., 2023) at 0.25° × 0.3125° resolution and TM5-MP (Williams et al., 2017; Bucsela et al., 2013) at 1° × 1° resolution,

130 respectively. However, the L2 version 2.0 GEMS product used incorrect GEOS-Chem vertical coordinates. To eliminate differences caused by using different vertical shape factors, we replace the profiles in the GEMS and TROPOMI L2 products with identical GEOS-Chem model profiles extending from the surface to the stratopause. Yang et al. (2023) showed that GEOS-Chem successfully reproduces the vertical profiles of NO<sub>2</sub> and their diurnal variations observed over South Korea in the KORUS-AQ aircraft campaign, supporting the use of GEOS-Chem profiles in a common AMF calculation for GEMS and TROPOMI satellite retrievals in East Asia. We use monthly mean hourly profiles from a 0.25° × 0.3125° resolution simulation with GEOS-Chem version 13.0.0 (DOI: 10.5281/zenodo.4618180). Details on model configuration and emissions  
135 can be found in Lee et al. (2024).

Scattering weights are not provided in the GEMS L2 NO<sub>2</sub> product, therefore we use scattering weights calculated by VLIDORT using GEMS geometry and atmospheric conditions at 448 nm, which are provided in the GEMS L2 glyoxal product (National Institute of Environmental Research 2020a). The GEMS glyoxal algorithm uses a spectral fitting window of 433.0–461.5 nm (Ha et al., 2024), which sufficiently overlaps with the NO<sub>2</sub> fitting window (435–450 nm). The AMF for the GEMS total column can then be calculated using vertical shape factors from GEOS-Chem, following Eq. (1). The  
140 TROPOMI L2 product reports averaging kernels  $A(z)$ , which normalize the scattering weights to the reported AMF (Eskes and Boersma, 2003).

$$A(z) = \frac{w(z)}{\text{AMF}} \quad (2)$$

The AMF for the TROPOMI total column can then be calculated from the GEOS-Chem vertical shape factors as follows:

$$145 \quad \text{AMF}' = \text{AMF} \int_0^{\text{TOA}} A(z) S(z) dz, \quad (3)$$

where AMF is from the L2 product and AMF' is the reprocessed value using GEOS-Chem vertical shape factors. The TROPOMI product reports  $A(z)$  for 34 layers, corresponding to the TM5-MP vertical grid, and we interpolate the values to the 47-layer vertical grid of GEOS-Chem. GEMS pixels with AlgorithmQualityFlags > 112, AMFQualityFlags > 64, FinalAlgorithmFlags > 1, and TROPOMI pixels with qa\_value < 0.75 are filtered out as per quality control  
150 recommendations. No other filtering is used. We apply area-weighted regridding to the filtered satellite products and use hourly gridded data at 0.25° × 0.3125° resolution with cloud fraction ≤ 0.3 and SZA ≤ 70° for the remainder of this study.

Figure 1 shows how the reprocessing of AMFs modifies the TROPOMI and GEMS NO<sub>2</sub> VCDs compared to the operational L2 products. In what follows, we denote the operational L2 products as “TROPOMI L2” and “GEMS L2”, and the products reprocessed with GEOS-Chem vertical profiles as “Reprocessed TROPOMI” and “Reprocessed GEMS”. The reprocessing  
155 increases TROPOMI in the Northeast Asia source regions including eastern China, South Korea, and Japan. GEMS decreases over eastern China and increases elsewhere.

Figure 2 compares NO<sub>2</sub> VCDs from the L2 and reprocessed products for the ensemble of GEMS and TROPOMI daily data sampled at the overpass time of TROPOMI. For the L2 products we find a negative normalized mean bias (NMB) of −14%

in GEMS compared to TROPOMI due to lower background values, but source regions are higher in GEMS. Reprocessing to common prior profiles greatly reduces GEMS-TROPOMI differences except in the background where some differences increase.

Figure 3a compares the mean seasonal variations of Pandora and satellite NO<sub>2</sub> VCDs averaged over the 16 Pandora stations in Northeast Asia. The VCDs are maximum in winter and minimum in summer, reflecting the lifetime of NO<sub>x</sub> against photochemical oxidation. The operational TROPOMI L2 product has a -16% NMB relative to the Pandora data that is reduced to 7% when reprocessed with GEOS-Chem vertical profiles. The operational GEMS L2 product has a 23% NMB relative to Pandora that is reduced to 7% when reprocessed with GEOS-Chem vertical profiles. The reprocessed TROPOMI and GEMS products are in close agreement, in contrast to the large differences between the TROPOMI L2 and GEMS L2 products, showing that much of the discrepancy in the L2 products stem from different vertical shape factors. Incorrect use of GEOS-Chem vertical coordinates in the L2 version 2.0 GEMS product will be corrected in the next operational product with the GEOS-Chem profiles used here for reprocessing. In the following section we correct the remaining discrepancies between the TROPOMI and GEMS reprocessed products using machine learning.

Figures 3b and 3c show the mean diurnal variations in the warm and cold seasons, comparing GEMS and Pandora. The Pandora data in the cold season increase over the course of the day due to daytime emissions, while the data in the warm season are minimum in early afternoon due to chemical loss (Yang et al., 2024). The operational GEMS L2 data feature a midday maximum in the cold season that is not seen in the Pandora data. Our reprocessed product is more consistent with the diurnal variation observed by Pandora. More detailed comparisons of diurnal variations in Pandora and GEMS are presented by Yang et al. (2024) for Beijing and Seoul.

#### 4 Bias correction in GEMS using machine learning

Here we construct a TROPOMI-corrected GEMS product by developing an ML model that can predict the differences,  $\Delta(\text{GEMS-TROPOMI})$ , remaining between GEMS and TROPOMI after reprocessing to common vertical profiles. TROPOMI is used as reference because of the greater maturity of its retrieval. The ML model uses as predictors the GEMS NO<sub>2</sub> VCD and the GEMS retrieval parameters provided in the L2 product including effective zenith angle (EZA), relative azimuth angle, aerosol optical depth, aerosol layer height, O<sub>3</sub> column amount, surface reflectance at 440 nm, single scattering albedo, cloud fraction, and cloud top pressure. EZA combines the geometric effects of SZA and VZA on the AMF, as defined by the geometric  $\text{AMF} = \sec(\text{EZA}) + 1$  in the absence of scattering (Palmer et al., 2001):

$$\sec(\text{EZA}) = \sec(\text{SZA}) + \sec(\text{VZA}) - 1. \quad (4)$$

TROPOMI observations are for a single time of day but extend off-track to viewing angles  $\pm 50^\circ$ , so that the collocated dataset covers EZA values ranging up to  $75^\circ$ . This allows us to build an ML model valid for a sufficient range of EZAs, as is necessary for application to GEMS observations over their full diurnal range.

Deleted: y

Deleted: relevant to GEMS observations at different times of day

We tested five ensemble method algorithms including both bagging (Random Forest, Extra Tree) and boosting (LightGBM, XGBoost, CatBoost) using the Fast and Lightweight AutoML Library (FLAML) (Wang et al., 2021). We separated collocated  $\Delta(\text{GEMS-TROPOMI})$  pairs into training (July and October 2022, January and April 2023) and test (rest of the collocated data for July 2022–June 2023) datasets. The average  $\text{NO}_2$  VCD from the test dataset is higher than the training data by 5% but the two datasets display similar spatial distributions. We trained the models to fit 7,489,498  $\Delta(\text{GEMS-TROPOMI})$  pairs (training data) for four months as representative of the four seasons, and found that the LightGBM algorithm has the best performance. We excluded  $\Delta(\text{GEMS-TROPOMI})$  data lying outside six times the interquartile range ( $6 \times \text{IQR}$ ; 0.1% of the training data) to avoid contamination by outliers.

Figure 4 compares observed and predicted differences for the test data. We conducted a Z-score transform to correct possible systematic biases associated with the LightGBM algorithm (Belitz and Stackelberg, 2021; Balasus et al., 2023). The  $R^2$  for the ML prediction is 0.51 and the root-mean-square-error (RMSE) is  $0.65 \times 10^{15}$  molecules  $\text{cm}^{-2}$ , which lies within the estimated single-retrieval errors of GEMS and TROPOMI  $\text{NO}_2$  of  $0.15\text{--}2.47 \times 10^{15}$  molecules  $\text{cm}^{-2}$  (Kim et al., 2020) and approximately  $0.5 \times 10^{15}$  molecules  $\text{cm}^{-2}$  (Van Geffen et al., 2022), respectively.

We produced a corrected GEMS product for the duration of the GEMS L2 version 2.0 record (November 2020 to present) by subtracting  $\Delta(\text{GEMS-TROPOMI})$  from the GEMS data previously reprocessed to the GEOS-Chem vertical profiles:

$$\text{GEMS}_{\text{corrected}} = \text{GEMS} - \Delta(\text{GEMS-TROPOMI}). \quad (5)$$

The ML calculation of  $\Delta(\text{GEMS-TROPOMI})$  requires only GEMS retrieval information and is therefore applied to all GEMS retrievals, not requiring collocation with TROPOMI.

Figure 5 compares TROPOMI, GEMS, and the corrected GEMS  $\text{NO}_2$  VCDs for the warm and cold seasons. The corrected GEMS product increases VCDs in the remote, ocean background in the southeastern part of the GEMS scan domain by up to 200% and decreases VCDs in Central Asia by up to 40%, regardless of season. However, corrections to the GEMS product in the polluted regions in Northeast Asia display different patterns during the warm and cold months. Figure 6 shows an enlarged view of the Northeast Asia domain along with observations from the Pandora stations. In the warm season, GEMS displays consistent 10% negative biases relative to TROPOMI in eastern parts of China and South Korea (Figure 6d), resulting in an upward correction. The GEMS bias in the cold season is much noisier and tends to be positive, resulting in downward correction (Figure 6j).

Comparison of the monthly mean variations of GEMS VCDs at the Pandora sites in Northeast Asia also shows that the ML model performs an upwards correction during May to August, and a larger downwards correction during other months, resulting in an overall low bias of  $\sim 5\%$  compared to TROPOMI (Figure 3a). However, we see from Figure 2 that the correction successfully reduces remaining residual differences between GEMS and TROPOMI ( $\text{NMB} = 0\%$ ) for the entire GEMS domain and increases consistency with the observed variability from TROPOMI ( $R^2 = 0.72$ ).

We can determine the contribution of each predictor variable to the model prediction using the SHapley Additive exPlanations (SHAP) analysis with the TreeExplainer method (Lundberg et al., 2020), as shown in Figure 7. The SHAP

**Deleted:** We can determine the contribution of each predictor variable to the model prediction using the SHapley Additive exPlanations (SHAP) analysis with the TreeExplainer method (Lundberg et al., 2020), as shown in Figure 4. The SHAP value can be interpreted as the relative importance of the predictor variable to the bias correction, where negative SHAP values indicate low biases in GEMS, and vice versa. Figure 4a shows that the GEMS  $\text{NO}_2$  VCD contributes to the largest corrections, followed by the EZA, while variables related to atmospheric scattering and surface reflectance are less important. Figure 4b shows that the corrections from  $\text{NO}_2$  VCD and EZA are strongly non-linear. The  $\text{NO}_2$  VCD drives the correction of the low bias in the ocean background and the high bias in polluted regions. EZA drives a correction for high biases at angles exceeding  $60^\circ$ . The dominant corrections from VCD and EZA might be viewed as reflecting a correction from the SCD, as we would have  $\text{SCD}/\text{VCD} = \sec(\text{EZA}) + 1$  in the absence of scattering. However, we found that using GEMS SCD as a predictor variable was less successful than using VCD.

**Deleted:** 5

**Deleted:** 6

**Deleted:** the

**Deleted:** in GEMS

**Moved (insertion) [1]**

**Deleted:** 7

**Deleted:** 7

**Deleted:** W

**Deleted:** also

**Formatted:** Space Before: 0 pt, After: 0 pt

value can be interpreted as the relative importance of the predictor variable to the bias correction, where negative SHAP values indicate low biases in GEMS, and vice versa. Figure 7a shows that the GEMS NO<sub>2</sub> VCD contributes the largest corrections, followed by the EZA, while variables related to atmospheric scattering and surface reflectance are less important. Figure 7b shows that the corrections from NO<sub>2</sub> VCD and EZA are strongly non-linear. The NO<sub>2</sub> VCD drives the correction of the low bias in the ocean background and the high bias in polluted regions. EZA drives a correction for high biases at angles exceeding 60°. The dominant corrections from VCD and EZA might be viewed as reflecting a correction from the SCD, as we would have  $SCD/VCD = \sec(EZA) + 1$  in the absence of scattering. However, we found that using GEMS SCD as a predictor variable was less successful than using VCD.

The effect of the correction on the diurnal profiles observed by GEMS at the Pandora sites is shown in Figure 3b-c. The correction in the warm season dampens the diurnal variability because EZA varies from 50° at local noon to 65° at 07:00 or 17:00 LT, a range limited by the constant VZA set by latitude. The corrected diurnal variability improves agreement with Pandora in late afternoon while degrading it in early morning. By contrast, the correction in the cold season decreases GEMS by similar increments for all hours of the day, resulting in no change in the diurnal profile but better agreement with Pandora. The lack of diurnal variability in the correction is because EZA varies over only a limited range. The VZA averages 44° for the Northeast Asia Pandora sites, and the SZA ranges from 52° at local noon to 65° at 08:00 or 16:00 LT, so that the EZA varies only from 60° to 68°.

## 5 Conclusions

We have presented an improved NO<sub>2</sub> vertical column density (VCD) product from the Geostationary Environment Monitoring Spectrometer (GEMS) by calibrating it to TROPOspheric Monitoring Instrument (TROPOMI) with a machine learning (ML) algorithm. A first step was to reprocess both GEMS and TROPOMI datasets to adopt common NO<sub>2</sub> vertical profiles and resulting air mass factors (AMFs) from the GEOS-Chem model. The second step was to correct the residual difference,  $\Delta(GEMS-TROPOMI)$ , with the ML model. The corrected GEMS product preserves the data density of GEMS, providing hourly daytime data over East/South Asia and neighboring oceans, and is consistent with TROPOMI. It is available for the duration of the GEMS record (November 2020 to present).

Reprocessing with a common AMF removed most of the differences between GEMS and TROPOMI operational L2 products. It also resulted in better agreement with the ground-based Pandora observations. Even after this reprocessing, GEMS displayed low biases compared to TROPOMI in polluted regions of eastern China and South Korea, as well as in the ocean background, and high biases in Central Asia.

We used the LightGBM ML algorithm to correct these remaining biases in GEMS relative to TROPOMI. We trained the ML model to fit collocated  $\Delta(GEMS-TROPOMI)$  pairs for four months (July and October 2022, January and April 2023) to GEMS NO<sub>2</sub> VCDs and GEMS retrieval parameters. This took advantage of the wide range of TROPOMI viewing angles to train the ML in a manner relevant to GEMS observations at different times of day. The ML was successful in correcting the

Formatted: English (US)

**Moved up [1]:** Figure 7 shows an enlarged view of the Northeast Asia domain along with observations from the Pandora stations. In the warm season, GEMS displays consistent 10% negative biases relative to TROPOMI in eastern parts of China and South Korea (Figure 7d), resulting in an upward correction. The GEMS bias in the cold season is much noisier and tends to be positive, resulting in downward correction.

Deleted: T

Deleted: makes the corrected GEMS agree better

Deleted: The correction in the warm season decreases GEMS values only in early morning and late afternoon, modifying the diurnal profile, but the comparison to Pandora is ambiguous. The Pandora data, observing the urban cores, may be less representative of the GEMS observations in summer than in winter when the NO<sub>x</sub> lifetime is longer and winds are stronger (Yang et al., 2024).

Deleted: in

Deleted: an

Deleted: including for GEMS diurnal profiles



remaining GEMS differences with TROPOMI. SHAP analysis showed that NO<sub>2</sub> VCD and effective zenith angle (EZA) were the predictor variables associated with largest corrections. ML correction increases VCDs in the remote ocean regions by up to 200% and decreases VCDs in Central Asia by up to 40%. GEMS values in NO<sub>x</sub> source regions of eastern China and South Korea increase by ~10% during the warm season but decrease during the cold season, resulting in better agreement with Pandora observations. The GEMS correction in these source regions is largest for early morning and late afternoon in the warm season, but is similar for all times of day in the cold season.

**Deleted:** the ocean background in GEMS

**Deleted:** , but is largest for early morning and late afternoon in the warm season.

Our corrected GEMS NO<sub>2</sub> product is designed to be consistent with the TROPOMI product, supporting the combined use of both datasets for analyses of East Asia air quality including NO<sub>x</sub> emissions and chemistry and their diurnal variations. Our approach of calibrating GEMS NO<sub>2</sub> observations to TROPOMI can be extended to other observed species (such as formaldehyde or glyoxal) and to other geostationary satellite instruments including TEMPO over North America and Sentinel-4 over Europe. This would produce consistent datasets across the geostationary air quality constellation with reference to a common TROPOMI calibration for global observing capability.

#### Data availability

GEMS L2, TROPOMI L2, and Pandora NO<sub>2</sub> products are available online through <https://nesc.nier.go.kr/en/html/index.do>, <https://dataspace.copernicus.eu/explore-data/data-collections/sentinel-data/sentinel-5p>, and <https://www.pandonia-global-network.org>, respectively. The corrected GEMS product from November 2020 to present will be available on Harvard Dataverse upon publication.

#### Author contributions

Original draft preparation, data processing, analysis, investigation, and visualization were done by YJO. DJJ and NB contributed to project conceptualization. Review and editing were done by DJJ, NB, HC, RJP, H-AK, and JK. LHY, JP, HL, GTL, and ESH provided additional resources and support in analysis.

#### Competing interests

The contact author has declared that none of the authors has any competing interests.

#### Financial support

This research was supported by the Samsung Advanced Institute of Technology.

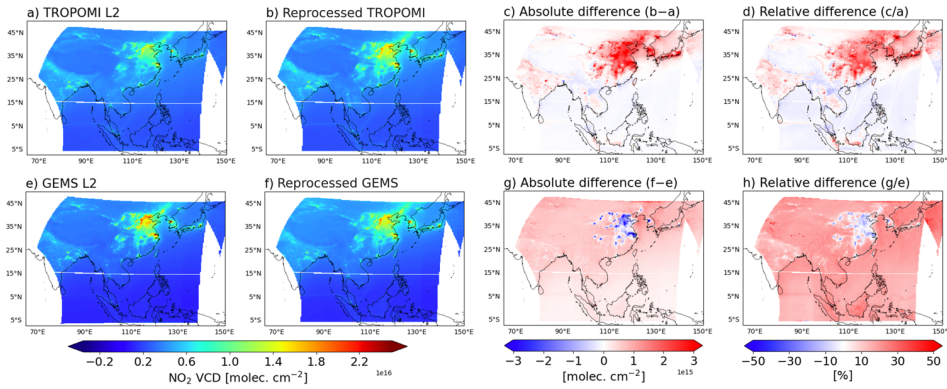
## References

- 330 Balasus, N., Jacob, D. J., Lorente, A., Maasakkers, J. D., Parker, R. J., Boesch, H., Chen, Z., Kelp, M. M., Nesser, H., and Varon, D. J.: A blended TROPOMI+GOSAT satellite data product for atmospheric methane using machine learning to correct retrieval biases, *Atmos. Meas. Tech. Discuss.*, 2023, 1-40, 10.5194/amt-2023-47, 2023.
- Beirle, S. and Wagner, T.: A new method for estimating megacity NO<sub>x</sub> emissions and lifetimes from satellite observations, *EGUsphere*, 2024, 1-21, 10.5194/egusphere-2023-3079, 2024.
- 335 Belitz, K. and Stackelberg, P. E.: Evaluation of six methods for correcting bias in estimates from ensemble tree machine learning regression models, *Environmental Modelling & Software*, 139, 105006, <https://doi.org/10.1016/j.envsoft.2021.105006>, 2021.
- Bey, I., Jacob, D. J., Yantosca, R. M., Logan, J. A., Field, B. D., Fiore, A. M., Li, Q., Liu, H. Y., Mickley, L. J., and Schultz, M. G.: Global modeling of tropospheric chemistry with assimilated meteorology: Model description and evaluation, *Journal of Geophysical Research: Atmospheres*, 106, 23073-23095, <https://doi.org/10.1029/2001JD000807>, 2001.
- 340 Boersma, K. F., Jacob, D. J., Eskes, H. J., Pinder, R. W., Wang, J., and van der A, R. J.: Intercomparison of SCIAMACHY and OMI tropospheric NO<sub>2</sub> columns: Observing the diurnal evolution of chemistry and emissions from space, *Journal of Geophysical Research: Atmospheres*, 113, <https://doi.org/10.1029/2007JD008816>, 2008.
- Bucsel, E. J., Krotkov, N. A., Celarier, E. A., Lamsal, L. N., Swartz, W. H., Bhartia, P. K., Boersma, K. F., Veefkind, J. P., Gleason, J. F., and Pickering, K. E.: A new stratospheric and tropospheric NO<sub>2</sub> retrieval algorithm for nadir-viewing satellite instruments: applications to OMI, *Atmos. Meas. Tech.*, 6, 2607-2626, 10.5194/amt-6-2607-2013, 2013.
- 345 Burrows, J. P., Weber, M., Buchwitz, M., Rozanov, V., Ladstätter-Weißmayer, A., Richter, A., DeBeek, R., Hoogen, R., Bramstedt, K., Eichmann, K.-U., Eisinger, M., and Perner, D.: The Global Ozone Monitoring Experiment (GOME): Mission Concept and First Scientific Results, *Journal of the Atmospheric Sciences*, 56, 151-175, [https://doi.org/10.1175/1520-0469\(1999\)056<0151:TGOMEG>2.0.CO;2](https://doi.org/10.1175/1520-0469(1999)056<0151:TGOMEG>2.0.CO;2), 1999.
- 350 Cai, K., Li, S., Lai, J., Xia, Y., Wang, Y., Hu, X., and Li, A.: Evaluation of TROPOMI and OMI Tropospheric NO<sub>2</sub> Products Using Measurements from MAX-DOAS and State-Controlled Stations in the Jiangsu Province of China, *Atmosphere*, 13, 886, 2022.
- The International GEOS-Chem User Community: geoschem/GCClassic: GEOS-Chem 13.0.0 (13.0.0) [dataset], <https://doi.org/10.5281/zenodo.4618180>, 2021.
- 355 Cooper, M. J., Martin, R. V., McLinden, C. A., and Brook, J. R.: Inferring ground-level nitrogen dioxide concentrations at fine spatial resolution applied to the TROPOMI satellite instrument, *Environmental Research Letters*, 15, 104013, 10.1088/1748-9326/aba3a5, 2020.
- Curier, R. L., Kranenburg, R., Segers, A. J. S., Timmermans, R. M. A., and Schaap, M.: Synergistic use of OMI NO<sub>2</sub> tropospheric columns and LOTOS-EUROS to evaluate the NO<sub>x</sub> emission trends across Europe, *Remote Sensing of Environment*, 149, 58-69, <https://doi.org/10.1016/j.rse.2014.03.032>, 2014.
- 360 Dang, R., Jacob, D. J., Shah, V., Eastham, S. D., Fritz, T. M., Mickley, L. J., Liu, T., Wang, Y., and Wang, J.: Background nitrogen dioxide (NO<sub>2</sub>) over the United States and its implications for satellite observations and trends: effects of nitrate photolysis, aircraft, and open fires, *Atmos. Chem. Phys.*, 23, 6271-6284, 10.5194/acp-23-6271-2023, 2023.
- 365 Douros, J., Eskes, H., van Geffen, J., Boersma, K. F., Compernelle, S., Pinardi, G., Blechschmidt, A. M., Peuch, V. H., Colette, A., and Veefkind, P.: Comparing Sentinel-5P TROPOMI NO<sub>2</sub> column observations with the CAMS regional air quality ensemble, *Geosci. Model Dev.*, 16, 509-534, 10.5194/gmd-16-509-2023, 2023.
- Duncan, B. N., Lamsal, L. N., Thompson, A. M., Yoshida, Y., Lu, Z., Streets, D. G., Hurwitz, M. M., and Pickering, K. E.: A space-based, high-resolution view of notable changes in urban NO<sub>x</sub> pollution around the world (2005–2014), *Journal of Geophysical Research: Atmospheres*, 121, 976-996, <https://doi.org/10.1002/2015JD024121>, 2016.
- 370 Eskes, H., van Geffen, J., Boersma, F., Eichmann, K.-U., Apituley, A., Pedernana, M., Sneep, M., Veefkind, J. P., and Loyola, D.: Sentinel-5 precursor/TROPOMI Level 2 Product User Manual Nitrogen Dioxide, 2022.
- Eskes, H. J. and Boersma, K. F.: Averaging kernels for DOAS total-column satellite retrievals, *Atmos. Chem. Phys.*, 3, 1285-1291, 10.5194/acp-3-1285-2003, 2003.
- 375 Geddes, J. A., Martin, R. V., Bucsel, E. J., McLinden, C. A., and Cunningham, D. J. M.: Stratosphere–troposphere separation of nitrogen dioxide columns from the TEMPO geostationary satellite instrument, *Atmos. Meas. Tech.*, 11, 6271-6287, 10.5194/amt-11-6271-2018, 2018.

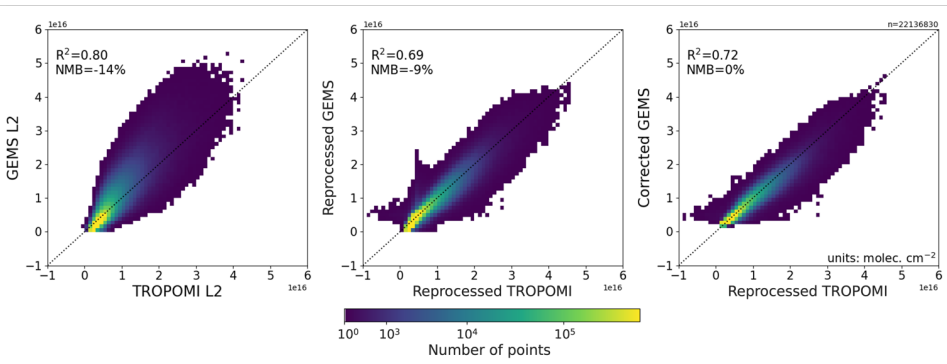
- Goldberg, D. L., Lu, Z., Streets, D. G., de Foy, B., Griffin, D., McLinden, C. A., Lamsal, L. N., Krotkov, N. A., and Eskes, H.: Enhanced Capabilities of TROPOMI NO<sub>2</sub>: Estimating NO<sub>x</sub> from North American Cities and Power Plants, *Environmental Science & Technology*, 53, 12594-12601, 10.1021/acs.est.9b04488, 2019.
- Gu, J., Liang, X., Song, S., Tian, Y., Chen, L., and Tao, J.: Evaluation of TROPOMI operational standard NO<sub>2</sub> column retrievals (from version 1.3 to 2.4) with OMNO2 and QA4ECV OMI observations over China, *EGUsphere*, 2023, 1-40, 10.5194/egusphere-2023-175, 2023.
- Ha, E. S., Park, R. J., Kwon, H. A., Lee, G. T., Lee, S. D., Shin, S., Lee, D. W., Hong, H., Lerot, C., De Smedt, I., Hendrick, F., and Irie, H.: First evaluation of the GEMS glyoxal products against TROPOMI and ground-based measurements, *EGUsphere*, 2024, 1-25, 10.5194/egusphere-2024-589, 2024.
- Herman, J., Cede, A., Spinei, E., Mount, G., Tzortziou, M., and Abuhassan, N.: NO<sub>2</sub> column amounts from ground-based Pandora and MFDOAS spectrometers using the direct-sun DOAS technique: Intercomparisons and application to OMI validation, *Journal of Geophysical Research: Atmospheres*, 114, <https://doi.org/10.1029/2009JD011848>, 2009.
- Herman, J., Abuhassan, N., Kim, J., Kim, J., Dubey, M., Raponi, M., and Tzortziou, M.: Underestimation of column NO<sub>2</sub> amounts from the OMI satellite compared to diurnally varying ground-based retrievals from multiple PANDORA spectrometer instruments, *Atmos. Meas. Tech.*, 12, 5593-5612, 10.5194/amt-12-5593-2019, 2019.
- Hong, H., Lee, H., Kim, J., Jeong, U., Ryu, J., and Lee, D. S.: Investigation of Simultaneous Effects of Aerosol Properties and Aerosol Peak Height on the Air Mass Factors for Space-Borne NO<sub>2</sub> Retrievals, *Remote. Sens.*, 9, 208, 2017.
- Ingmann, P., Veihelmann, B., Langen, J., Lamarre, D., Stark, H., and Courrèges-Lacoste, G. B.: Requirements for the GMES Atmosphere Service and ESA's implementation concept: Sentinels-4/-5 and -5p, *Remote Sensing of Environment*, 120, 58-69, <https://doi.org/10.1016/j.rse.2012.01.023>, 2012.
- Kim, J., Jeong, U., Ahn, M.-H., Kim, J. H., Park, R. J., Lee, H., Song, C. H., Choi, Y.-S., Lee, K.-H., Yoo, J.-M., Jeong, M.-J., Park, S. K., Lee, K.-M., Song, C.-K., Kim, S.-W., Kim, Y. J., Kim, S.-W., Kim, M., Go, S., Liu, X., Chance, K., Chan Miller, C., Al-Saadi, J., Veihelmann, B., Bhartia, P. K., Torres, O., Abad, G. G., Haffner, D. P., Ko, D. H., Lee, S. H., Woo, J.-H., Chong, H., Park, S. S., Nicks, D., Choi, W. J., Moon, K.-J., Cho, A., Yoon, J., Kim, S.-k., Hong, H., Lee, K., Lee, H., Lee, S., Choi, M., Veeckind, P., Levelt, P. F., Edwards, D. P., Kang, M., Eo, M., Bak, J., Baek, K., Kwon, H.-A., Yang, J., Park, J., Han, K. M., Kim, B.-R., Shin, H.-W., Choi, H., Lee, E., Chong, J., Cha, Y., Koo, J.-H., Irie, H., Hayashida, S., Kasai, Y., Kanaya, Y., Liu, C., Lin, J., Crawford, J. H., Carmichael, G. R., Newchurch, M. J., Lefter, B. L., Herman, J. R., Swap, R. J., Lau, A. K. H., Kurosu, T. P., Jaross, G., Ahlers, B., Dobber, M., McElroy, C. T., and Choi, Y.: New Era of Air Quality Monitoring from Space: Geostationary Environment Monitoring Spectrometer (GEMS), *Bulletin of the American Meteorological Society*, 101, E1-E22, <https://doi.org/10.1175/BAMS-D-18-0013.1>, 2020.
- Kim, S., Kim, D., Hong, H., Chang, L. S., Lee, H., Kim, D. R., Kim, D., Yu, J. A., Lee, D., Jeong, U., Song, C. K., Kim, S. W., Park, S. S., Kim, J., Hanisco, T. F., Park, J., Choi, W., and Lee, K.: First-time comparison between NO<sub>2</sub> vertical columns from GEMS and Pandora measurements, *Atmos. Meas. Tech. Discuss.*, 2023, 1-22, 10.5194/amt-2023-11, 2023.
- Knowland, K. E., Keller, C. A., Wales, P. A., Wargan, K., Coy, L., Johnson, M. S., Liu, J., Lucchesi, R. A., Eastham, S. D., Fleming, E., Liang, Q., Leblanc, T., Livesey, N. J., Walker, K. A., Ott, L. E., and Pawson, S.: NASA GEOS Composition Forecast Modeling System GEOS-CF v1.0: Stratospheric Composition, *Journal of Advances in Modeling Earth Systems*, 14, e2021MS002852, <https://doi.org/10.1029/2021MS002852>, 2022.
- Kwon, H. A., Park, R. J., González Abad, G., Chance, K., Kurosu, T. P., Kim, J., De Smedt, I., Van Roozendael, M., Peters, E., and Burrows, J.: Description of a formaldehyde retrieval algorithm for the Geostationary Environment Monitoring Spectrometer (GEMS), *Atmos. Meas. Tech.*, 12, 3551-3571, 10.5194/amt-12-3551-2019, 2019.
- Lambert, J.-C., Keppens, A., Compernelle, S., Eichmann, K.-U., Graaf, M. d., Hubert, D., Langerock, B., Ludewig, A., Sha, M. K., Verhoelst, T., Wagner, T., Ahn, C., Argyrouli, A., Balis, D., Chan, K. L., Coldewey-Egbers, M., Smedt, I. D., Eskes, H., Fjærraa, A. M., Garane, K., Gleason, J. F., Goutail, F., Granville, J., Hedelt, P., Ahn, C., Heue, K.-P., Jaross, G., Kleipool, Q., Koukouli, M., Lutz, R., Velarte, M. C. M., Michailidis, K., Nanda, S., Niemeijer, S., Pazmiño, A., Pinardi, G., Richter, A., Rozemeijer, N., Sneep, M., Zweers, D. S., Theys, N., Tilstra, G., Torres, O., Valks, P., Geffen, J. v., Vigouroux, C., Wang, P., and Weber, M.: Quarterly Validation Report of the Copernicus Sentinel-5 Precursor Operational Data Products #21: April 2018 – November 2023., 194, 2023.
- Lamsal, L. N., Duncan, B. N., Yoshida, Y., Krotkov, N. A., Pickering, K. E., Streets, D. G., and Lu, Z.: U.S. NO<sub>2</sub> trends (2005–2013): EPA Air Quality System (AQS) data versus improved observations from the Ozone Monitoring Instrument (OMI), *Atmospheric Environment*, 110, 130-143, <https://doi.org/10.1016/j.atmosenv.2015.03.055>, 2015.

- Lee, G. T., Park, R. J., Kwon, H. A., Ha, E. S., Lee, S. D., Shin, S., Ahn, M. H., Kang, M., Choi, Y. S., Kim, G., Lee, D. W., Kim, D. R., Hong, H., Langerock, B., Vigouroux, C., Lerot, C., Hendrick, F., Pinardi, G., De Smedt, I., Van Roozendael, M., Wang, P., Chong, H., Cho, Y., and Kim, J.: First evaluation of the GEMS formaldehyde retrieval algorithm against TROPOMI and ground-based column measurements during the in-orbit test period, *EGUsphere*, 2023, 1-33, 10.5194/egusphere-2023-1918, 2024.
- Levelt, P. F., Oord, G. H. J. v. d., Dobber, M. R., Malkki, A., Huib, V., Johan de, V., Stammes, P., Lundell, J. O. V., and Saari, H.: The ozone monitoring instrument, *IEEE Transactions on Geoscience and Remote Sensing*, 44, 1093-1101, 10.1109/TGRS.2006.872333, 2006.
- Li, Y., Xing, C., Peng, H., Song, Y., Zhang, C., Xue, J., Niu, X., and Liu, C.: Long-term observations of NO<sub>2</sub> using GEMS in China: Validations and regional transport, *Science of The Total Environment*, 904, 166762, <https://doi.org/10.1016/j.scitotenv.2023.166762>, 2023.
- Liu, F., Beirle, S., Zhang, Q., van der A, R. J., Zheng, B., Tong, D., and He, K.: NO<sub>x</sub> emission trends over Chinese cities estimated from OMI observations during 2005 to 2015, *Atmos. Chem. Phys.*, 17, 9261-9275, 10.5194/acp-17-9261-2017, 2017.
- Lundberg, S. M., Erion, G., Chen, H., DeGrave, A., Prutkin, J. M., Nair, B., Katz, R., Himmelfarb, J., Bansal, N., and Lee, S.-I.: From local explanations to global understanding with explainable AI for trees, *Nature Machine Intelligence*, 2, 56-67, 10.1038/s42256-019-0138-9, 2020.
- Martin, R. V., Jacob, D. J., Chance, K., Kurosu, T. P., Palmer, P. I., and Evans, M. J.: Global inventory of nitrogen oxide emissions constrained by space-based observations of NO<sub>2</sub> columns, *Journal of Geophysical Research: Atmospheres*, 108, <https://doi.org/10.1029/2003JD003453>, 2003.
- Miyazaki, K., Eskes, H., Sudo, K., Boersma, K. F., Bowman, K., and Kanaya, Y.: Decadal changes in global surface NO<sub>x</sub> emissions from multi-constituent satellite data assimilation, *Atmos. Chem. Phys.*, 17, 807-837, 10.5194/acp-17-807-2017, 2017.
- Munro, R., Lang, R., Klaes, D., Poli, G., Retscher, C., Lindstrot, R., Huckle, R., Lacan, A., Grzegorski, M., Holdak, A., Kokhanovsky, A., Livschitz, J., and Eisinger, M.: The GOME-2 instrument on the Metop series of satellites: instrument design, calibration, and level 1 data processing – an overview, *Atmos. Meas. Tech.*, 9, 1279-1301, 10.5194/amt-9-1279-2016, 2016.
- Palmer, P. I., Jacob, D. J., Chance, K., Martin, R. V., Spurr, R. J. D., Kurosu, T. P., Bey, I., Yantosca, R., Fiore, A., and Li, Q.: Air mass factor formulation for spectroscopic measurements from satellites: Application to formaldehyde retrievals from the Global Ozone Monitoring Experiment, *Journal of Geophysical Research: Atmospheres*, 106, 14539-14550, <https://doi.org/10.1029/2000JD900772>, 2001.
- Park, J., Park, J.-S., Santana Díaz, D., Gebetsberger, M., Mueller, M., Shalaby, L., Tiefengraber, M., Kim, H.-J., Park, S. S., Song, C.-K., and Kim, S.-W.: Spatiotemporal inhomogeneity of total column NO<sub>2</sub> in a polluted urban area inferred from TROPOMI and Pandora intercomparisons, *GIScience & Remote Sensing*, 59, 354-373, 10.1080/15481603.2022.2026640, 2022.
- Pinardi, G., Van Roozendael, M., Hendrick, F., Theys, N., Abuhassan, N., Bais, A., Boersma, F., Cede, A., Chong, J., Donner, S., Drosoglou, T., Dzhola, A., Eskes, H., Frieß, U., Granville, J., Herman, J. R., Holla, R., Hovila, J., Irie, H., Kanaya, Y., Karagkiozidis, D., Kouremeti, N., Lambert, J. C., Ma, J., Peters, E., PETERS, A., Postylyakov, O., Richter, A., Remmers, J., Takashima, H., Tiefengraber, M., Valks, P., Vlemmix, T., Wagner, T., and Wittrock, F.: Validation of tropospheric NO<sub>2</sub> column measurements of GOME-2A and OMI using MAX-DOAS and direct sun network observations, *Atmos. Meas. Tech.*, 13, 6141-6174, 10.5194/amt-13-6141-2020, 2020.
- Platt, U.: Differential Optical Absorption Spectroscopy (DOAS), in: *Air monitoring by spectroscopic techniques*, edited by Sigrist, M. W., 127–76, <https://doi.org/10.1002/9780470027318.a0706>, 1994.
- National Institute of Environmental Research (NIER): Geostationary Environment Monitoring Spectrometer (GEMS) Algorithm Theoretical Basis Document VOC (HCHO/CHOCHO) Retrieval Algorithm, 2020a.
- National Institute of Environmental Research (NIER): Geostationary Environment Monitoring Spectrometer (GEMS) Algorithm Theoretical Basis Document NO<sub>2</sub> Retrieval Algorithm, 2020b.
- Spurr, R. and Christi, M.: On the generation of atmospheric property Jacobians from the (V)LIDORT linearized radiative transfer models, *Journal of Quantitative Spectroscopy and Radiative Transfer*, 142, 109-115, <https://doi.org/10.1016/j.jqsrt.2014.03.011>, 2014.

- Stammes, P.: Spectral radiance modelling in the UV-visible range, 2001.
- Travis, K., Jacob, D., Fisher, J., Kim, P., Marais, E., Zhu, L., Yu, K., Miller, C., Yantosca, R., Sulprizio, M., Thompson, A., Wennberg, P., Crounse, J., Clair, J., Cohen, R., Laughner, J., Dibb, J., Hall, S., Ullmann, K., and Zhou, X.: Why do models overestimate surface ozone in the Southeast United States?, *Atmospheric Chemistry and Physics*, 16, 13561-13577, 10.5194/acp-16-13561-2016, 2016.
- Valin, L. C., Russell, A. R., and Cohen, R. C.: Variations of OH radical in an urban plume inferred from NO<sub>2</sub> column measurements, *Geophysical Research Letters*, 40, 1856-1860, <https://doi.org/10.1002/grl.50267>, 2013.
- van Geffen, J. H. G. M., Eskes, H. J., Boersma, K. F., and Veefkind, J. P.: TROPOMI ATBD of the total and tropospheric NO<sub>2</sub> data products, 2022.
- Veefkind, J. P., Aben, I., McMullan, K., Förster, H., de Vries, J., Otter, G., Claas, J., Eskes, H. J., de Haan, J. F., Kleipool, Q., van Weele, M., Hasekamp, O., Hoogeveen, R., Landgraf, J., Snel, R., Tol, P., Ingmann, P., Voors, R., Kruizinga, B., Vink, R., Visser, H., and Levelt, P. F.: TROPOMI on the ESA Sentinel-5 Precursor: A GMES mission for global observations of the atmospheric composition for climate, air quality and ozone layer applications, *Remote Sensing of Environment*, 120, 70-83, <https://doi.org/10.1016/j.rse.2011.09.027>, 2012.
- Wang, C., Wang, T., Wang, P., and Rakitin, V.: Comparison and Validation of TROPOMI and OMI NO<sub>2</sub> Observations over China, *Atmosphere*, 11, 636, 2020.
- Wang, C., Wu, Q., Weimer, M., and Zhu, E.: Flam1: A fast and lightweight automl library, *Proceedings of Machine Learning and Systems*, 3, 434-447, 2021.
- Williams, J. E., Boersma, K. F., Le Sager, P., and Verstraeten, W. W.: The high-resolution version of TM5-MP for optimized satellite retrievals: description and validation, *Geosci. Model Dev.*, 10, 721-750, 10.5194/gmd-10-721-2017, 2017.
- Yang, L. H., Jacob, D. J., Colombi, N. K., Zhai, S., Bates, K. H., Shah, V., Beaudry, E., Yantosca, R. M., Lin, H., Brewer, J. F., Chong, H., Travis, K. R., Crawford, J. H., Lamsal, L. N., Koo, J. H., and Kim, J.: Tropospheric NO<sub>2</sub> vertical profiles over South Korea and their relation to oxidant chemistry: implications for geostationary satellite retrievals and the observation of NO<sub>2</sub> diurnal variation from space, *Atmos. Chem. Phys.*, 23, 2465-2481, 10.5194/acp-23-2465-2023, 2023.
- Yang, L. H., Jacob, D. J., Dang, R., Oak, Y. J., Lin, H., Kim, J., Zhai, S., Colombi, N. K., Pendergrass, D. C., Beaudry, E., Shah, V., Feng, X., Yantosca, R. M., Chong, H., Park, J., Lee, H., Lee, W. J., Kim, S., Kim, E., Travis, K. R., Crawford, J. H., and Liao, H.: Interpreting GEMS geostationary satellite observations of the diurnal variation of nitrogen dioxide (NO<sub>2</sub>) over East Asia, *EGUsphere*, 2023, 1-25, 10.5194/egusphere-2023-2979, 2024.
- Zhang, Y., Lin, J., Kim, J., Lee, H., Park, J., Hong, H., Van Roozendaal, M., Hendrick, F., Wang, T., Wang, P., He, Q., Qin, K., Choi, Y., Kanaya, Y., Xu, J., Xie, P., Tian, X., Zhang, S., Wang, S., Spurr, R., Chen, L., Kong, H., and Liu, M.: POMINO-GEMS: A Research Product for Tropospheric NO<sub>2</sub> Columns from Geostationary Environment Monitoring Spectrometer, *Atmos. Meas. Tech. Discuss.*, 2023, 1-28, 10.5194/amt-2023-46, 2023.
- Zoogman, P., Liu, X., Suleiman, R. M., Pennington, W. F., Flittner, D. E., Al-Saadi, J. A., Hilton, B. B., Nicks, D. K., Newchurch, M. J., Carr, J. L., Janz, S. J., Andraschko, M. R., Arola, A., Baker, B. D., Canova, B. P., Chan Miller, C., Cohen, R. C., Davis, J. E., Dussault, M. E., Edwards, D. P., Fishman, J., Ghulam, A., González Abad, G., Grutter, M., Herman, J. R., Houck, J., Jacob, D. J., Joiner, J., Kerridge, B. J., Kim, J., Krotkov, N. A., Lamsal, L., Li, C., Lindfors, A., Martin, R. V., McElroy, C. T., McLinden, C., Natraj, V., Neil, D. O., Nowlan, C. R., O'Sullivan, E. J., Palmer, P. I., Pierce, R. B., Pippin, M. R., Saiz-Lopez, A., Spurr, R. J. D., Szykman, J. J., Torres, O., Veefkind, J. P., Veihelmann, B., Wang, H., Wang, J., and Chance, K.: Tropospheric emissions: Monitoring of pollution (TEMPO), *Journal of Quantitative Spectroscopy and Radiative Transfer*, 186, 17-39, <https://doi.org/10.1016/j.jqsrt.2016.05.008>, 2017.



520 Figure 1: NO<sub>2</sub> total vertical column densities (VCDs) from TROPOMI and GEMS. Values are averages for July 2022–June 2023 sampled at the overpass time of TROPOMI (13:30 local time; LT). The top panels show the TROPOMI operational product (L2), our product reprocessed with GEOS-Chem NO<sub>2</sub> vertical profiles, and the absolute and relative differences between the two. The lower panels show the same for GEMS.



525 Figure 2: Scatterplot comparison of NO<sub>2</sub> total VCDs from TROPOMI and GEMS. Individual points are daily data for July 2022–June 2023 on the 0.25° × 0.3125° grid sampled at the overpass time of TROPOMI. The left panel compares the operational TROPOMI and GEMS products and the middle panel compares our reprocessed products with GEOS-Chem NO<sub>2</sub> vertical profiles, respectively. The right panel compares the reprocessed TROPOMI product with the GEMS data corrected for residual differences with TROPOMI using machine learning (ML) (Section 4). Colorscale shows density of points. The dashed line indicates the 1:1 line. Coefficient of determination ( $R^2$ ) and normalized mean bias ( $NMB = \frac{\sum(GEMS - TROPOMI)}{\sum TROPOMI} \times 100\%$ ) are given inset. **Negative TROPOMI values reflect noise in the SCD spectral fitting. The GEMS L2 product has no negative values.**

530

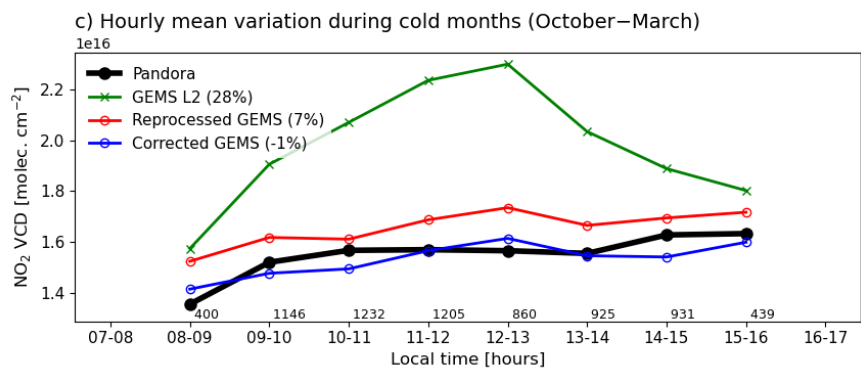
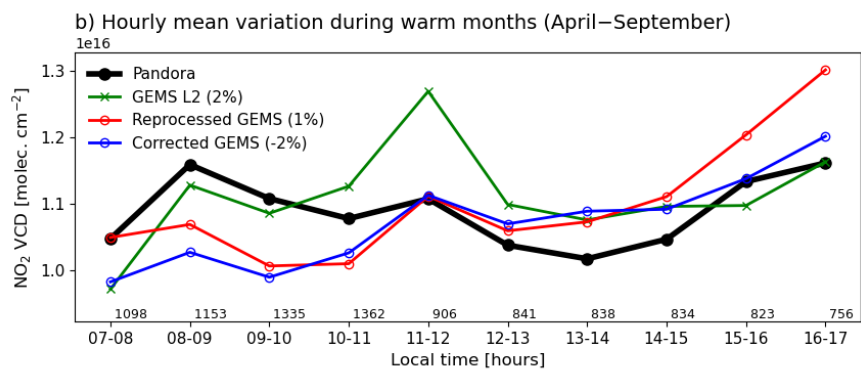
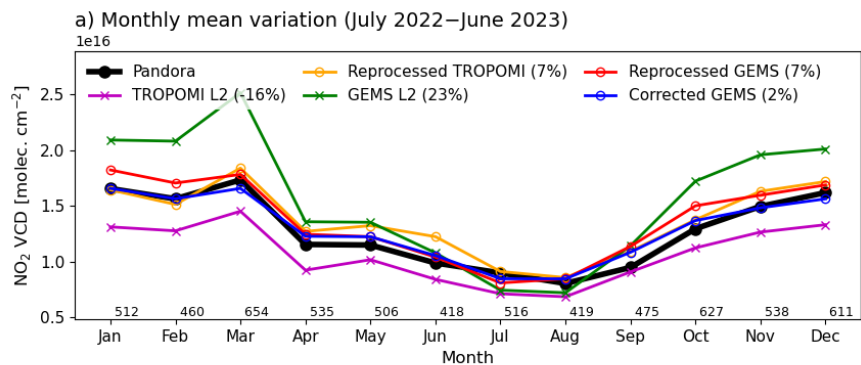


Figure 3: Seasonal and diurnal variations of NO<sub>2</sub> total VCDs from Pandora, TROPOMI, and GEMS averaged at 16 Pandora stations in Northeast Asia over July 2022–June 2023. TROPOMI and GEMS data are shown for the operational L2 products, and the products reprocessed with GEOS-Chem NO<sub>2</sub> vertical profiles. Also shown is the GEMS product corrected for residual differences with TROPOMI using ML (Section 4). Seasonal variations in the top panel are for the TROPOMI overpass time (13:30 LT). Diurnal variations in the middle and bottom panels are only for Pandora and GEMS and are shown for April–September and October–March. NMB relative to Pandora ( $NMB = \frac{\sum(Satellite - Pandora)}{\sum Pandora} \times 100\%$ ) are given inset. The numbers of observations for each month and hour are indicated.

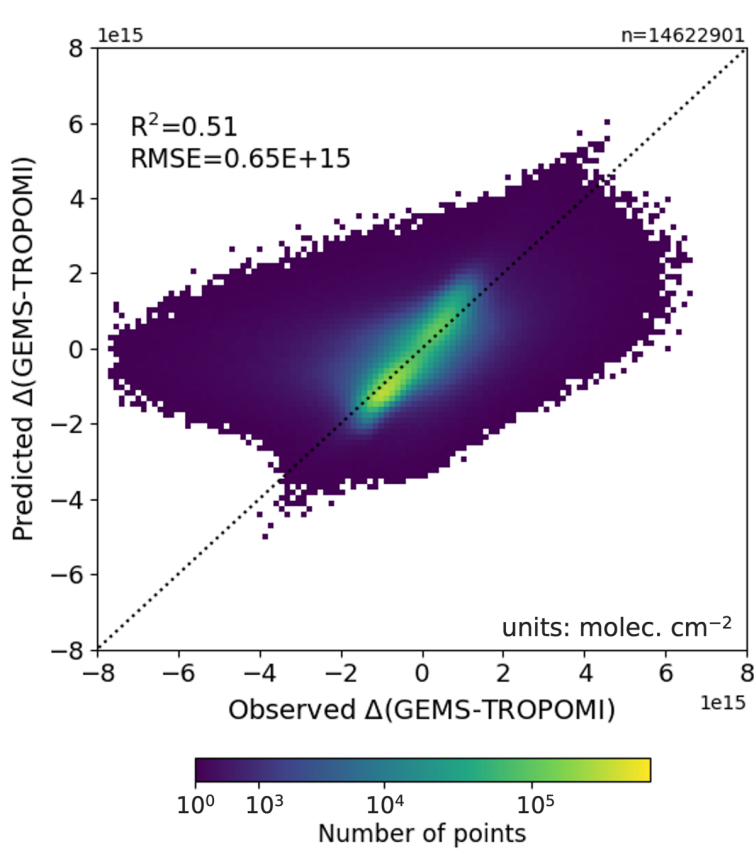
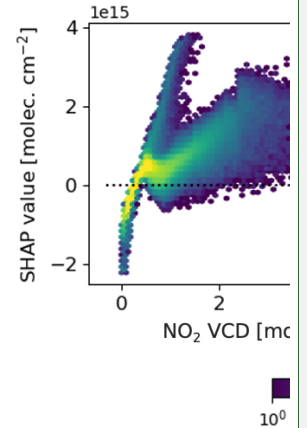


Figure 4: Predicted versus observed  $\Delta(GEMS-TROPOMI)$  in the test dataset. Colorscale shows density of points. The dashed line indicates the 1:1 line.  $R^2$  and root mean square error (RMSE) are given inset.

a) SHAP analysis of pred

- NO<sub>2</sub> VCD -
- Effective Zenith Angle -
- Cloud Pressure -
- Single Scattering Albedo -
- O<sub>3</sub> Column -
- Relative Azimuth Angle -
- Surface Reflectance -
- Aerosol Optical Depth -
- Aerosol Layer Height -
- Cloud Fraction -

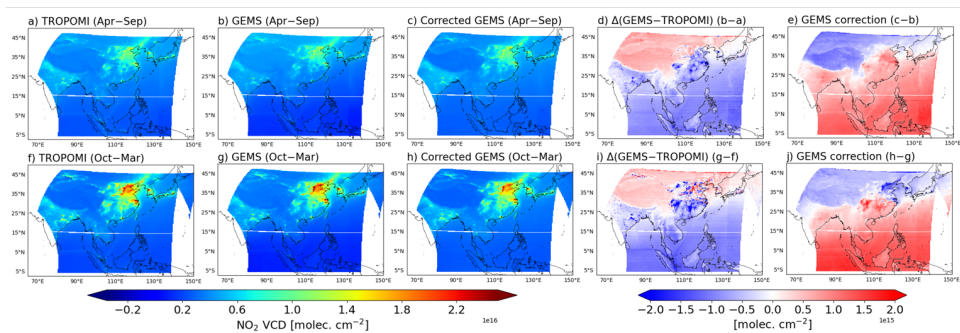
b) SHAP contribution to



Moved down [2]:

Deleted: 5

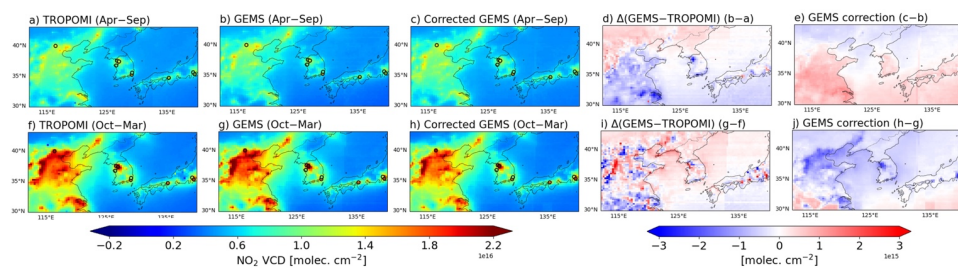




560

**Figure 5:** Comparison of TROPOMI, GEMS, and corrected GEMS  $\text{NO}_2$  products in the GEMS scan domain. (a-c)  $\text{NO}_2$  total VCDs averaged for April-September at the TROPOMI overpass time. The TROPOMI and GEMS data have been reprocessed to common GEOS-Chem vertical profiles for the observation scenes. (d)  $\Delta(\text{GEMS-TROPOMI})$  for April-September. (e) Correction to the GEMS product for April-September. (f-j) Same as panels (a-e) but for October-March.

Deleted: 6



565

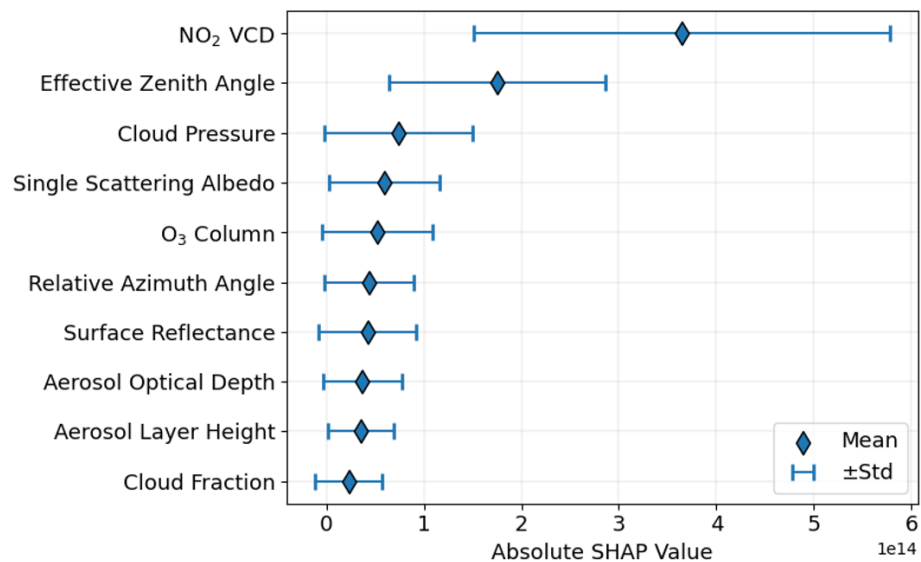
**Figure 6:** Same as Figure 5 but in the Northeast Asia domain with Pandora observations shown as circles. Colorscales are different from Figure 5.

Deleted: 7

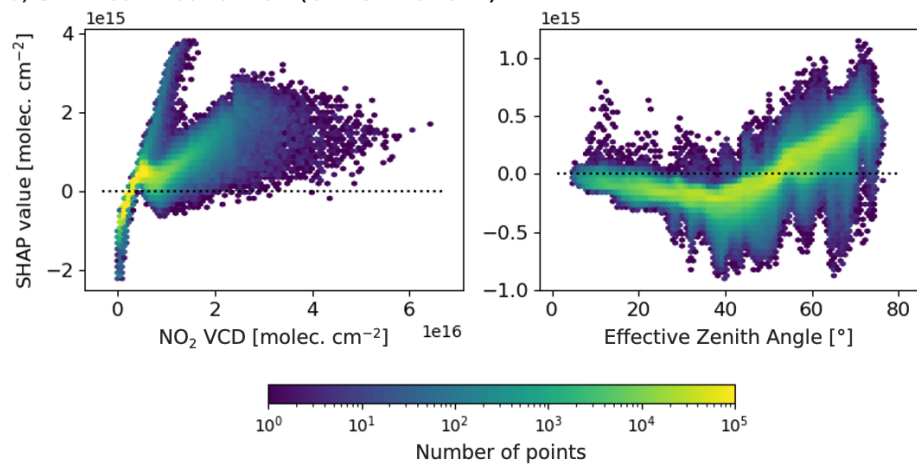
Deleted: 6

Deleted: 6

a) SHAP analysis of predictor variables



b) SHAP contribution to  $\Delta(\text{GEMS-TROPOMI})$



Moved (insertion) [2]

575

Figure 7: SHAP analysis for predictors of GEMS-TROPOMI differences,  $\Delta(\text{GEMS-TROPOMI})$ , in the ML training dataset. (a) SHAP analysis results ranking the predictor variables in order of their contributions to the fit. (b) SHAP contribution to  $\Delta(\text{GEMS-TROPOMI})$  from GEMS  $\text{NO}_2$  VCD and effective zenith angle (EZA). Color scale shows density of points.

Deleted: 4

Formatted: Caption

Deleted: ¶